CELL BIOLOGY

JLP-centrosome is essential for the microtubule-mediated nucleocytoplasmic transport induced by extracellular stimuli

Clement M. Lee[1]*, Ken Aizawa[1], Joshua Jiang[1], Sam K. P. Kung[2], Rinku Jain[3]

JLP belongs to the JIP family whose members serve as scaffolding proteins that link motor proteins and their cargo for intracellular transport. Although JLP is mainly cytoplasmic, it accumulates as a focus in the perinuclear region when stimulated by extracellular stimuli. Focus formation, which changes the nucleus shape and concentrates the nuclear pores, depends on p38MAPK activation and the dynein retrograde motor protein complex. Extracellular stimuli trigger the tethering of PLK1 to the centrosome by JLP, leading to centrosome maturation and microtubule array formation. The centrosome localization domain of JLP is important for the binding of the centrosome and the formation of the JLP focus and the microtubule array. Furthermore, the formation of the JLP focus and the microtubule array is interdependent and important for the transport of NF-κB p65 to the nucleus and its unloading therein. In conclusion, JLP exhibits multiple functions in the nuclear translocation of NF-κB p65.

INTRODUCTION

The scaffolding protein JLP [JNK (c-Jun N-terminal kinase)–associated leucine zipper protein] is one of the JIP (JNK interacting protein) family members (*1*, *2*). JLP interacts with cytoplasmic proteins such as JNK, p38 mitogen-activated protein kinase (p38MAPK), their upstream kinases, SCG10, $G_{\alpha 13}$, KLC1, and CDO, as well as nuclear transcription factors c-MYC and MAX (*1*, *3*–*6*). JLP tethers JNK/p38MAPK and their upstream kinases to form signaling cascades (*1*), and JNK and p38MAPK are involved in mediating the responses of various extracellular stress stimuli and proinflammatory cytokines (*7*). Furthermore, JLP associates with the anterograde and retrograde motor proteins kinesin-1 and dynein, respectively, which move in opposite directions along microtubules (MTs) (*5*, *8*–*10*).

Centrosomes are organelles located in the perinuclear region and involved in nucleating MTs during the formation of interphase, mitotic, and meiotic asters, giving rise to arrays of MTs (*11*). Each centrosome consists of two centrioles and various proteins in the pericentriolar material (PCM), including pericentrin and γ-tubulin (*12*). At the onset of mitosis, PCM recruits various proteins to organize an array of MTs. Centrosome maturation is initiated by Polo-like kinase 1 (PLK1)–mediated phosphorylation of various proteins in PCM, including pericentrin (*12*).

Nuclear factor κB (NF-κB) is a transcription factor kept latent in the cytoplasm (*13*). It is aberrantly activated in various human cancers and involved in tumor growth, progression, and resistance to chemotherapy (*14*). When cells are stimulated by extracellular stimuli, the protein is transported to the nucleus to activate gene transcription. It is known that NF-κB nuclear translocation requires MTs (*15*) and the cytoplasmic dynein motor complex (*16*). It is also known that extracellular stimuli induce rearrangement of MTs, and MTs associate with NF-κB and modulate its activation (*15*). However, the mechanism of transport of NF-κB to the nucleus remains obscure. In the present study, we show that extracellular stimulation induces the formation of JLP foci in a p38MAPK-, MT-, and dynein-dependent manner. The JLP foci contain mature centrosomes that nucleate MT arrays to connect the cytoplasm and nucleus for the transport of NF-κB p65 to the nucleus.

[1]Department of Oncological Sciences, Icahn School of Medicine at Mount Sinai, New York, NY 10029, USA. [2]Department of Immunology College of Medicine, Faculty of Health Science, University of Manitoba, Winnipeg, Manitoba R3E 0T5, Canada. [3]Department of Pharmacological Sciences, Icahn School of Medicine at Mount Sinai, New York, NY 10029, USA.
*Corresponding author. Email: clement.lee@mssm.edu

RESULTS

JLP focus

JLP interacts with the extracellular signal–regulated kinases (ERKs) JNK and p38MAPK and is involved in their signaling (*1*, *17*). To examine the subcellular localization of JLP after stimulation by extracellular stimuli, we stimulated the cells with arsenite to induce the activation of JNK and p38MAPK, as well as pathways mediated by oxidative stress (*18*). The results in Fig. 1A show that after 20 min of arsenite treatment, JLP appeared as an intense focus spot (JLP focus). The results in Fig. 1B show that the formation of JLP focus is time-dependent. Similar results were also observed in various cell lines (Fig. 1C) and with various extracellular stress stimuli and proinflammatory cytokines, except interleukin-3 (IL-3), which does not signal through JNK and p38MAPK (Fig. 1D). The only exception was the cells in mitosis, where the nuclear envelope is dissolved, whereas all other cells showed the JLP focus formation upon stimulation. Together, the results suggest that JLP may be involved in signal transduction of extracellular stimuli. The specificity of the JLP antibody for endogenous and epitope-tagged JLP for immunofluorescence and Western blot analyses was confirmed in fig. S1.

p38MAPK mediates the JLP focus formation

The involvement of JLP in JNK and p38MAPK signaling also suggests that these proteins regulate JLP focus formation. To test this possibility, we preincubated cells with various inhibitors for 1 hour followed by stimulation with arsenite. The results in Fig. 2 (A and B) show that none of the inhibitors, including the JNK inhibitor, could ablate JLP focus formation. However, the p38MAPK inhibitor reduced the formation of JLP foci, indicating that p38MAPK is involved in mediating the process. Protein analyses show that the inhibitors did not alter the JLP levels in the cells (Fig. 2A). The inhibition of JLP foci formation was dose dependent (Fig. 2C). Even at 20 μM, none of

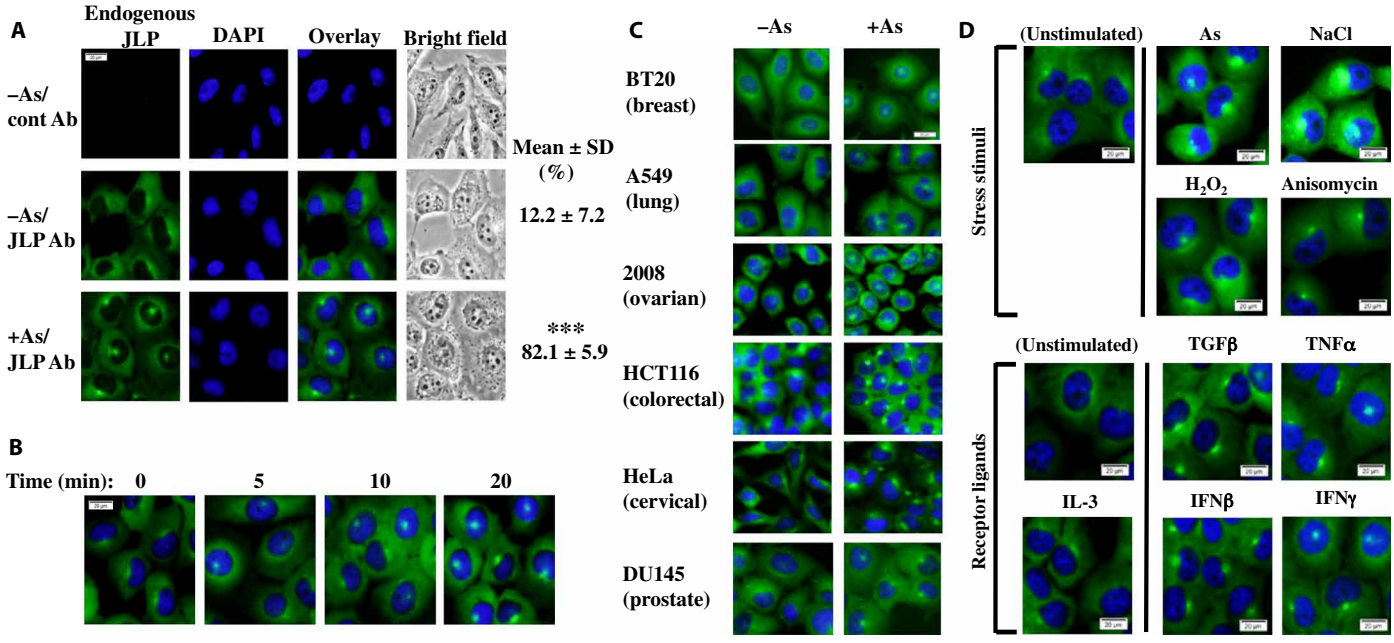

Fig. 1. JLP focus. (**A**) Induction of JLP foci by the arsenite treatment (0.5 mM for 30 min) in H1299 cells. They were fixed and stained with a control antibody (Ab) or the JLP antibody together with the DNA-intercalating dye 4′,6-diamidino-2-phenylindole (DAPI). The percentages of cells showing the JLP foci were scored and presented as mean ± SD % ($n = 3$). ***$P < 0.0005$ (as compared with untreated cells). (**B**) Time course of JLP localization after arsenite treatment. (**C**) Various cell lines were treated with or without arsenite (0.5 mM) for 30 min. (**D**) H1299 cells were treated with various stress stimuli or proinflammatory cytokines as indicated. Proliferation cytokine IL-3 served as a negative control. Scale bars, 20 μm.

the inhibitors, except the p38MAPK inhibitor, reduced the JLP focus intensities (Fig. 2C). Furthermore, when we expressed wild-type p38MAPK and its dominant-negative mutant (*19*) in the cells (Fig. 2D), mutant expression resulted in the reduction of JLP focus formation, suggesting that p38MAPK activity is required for robust JLP focus formation in response to external stimuli.

Dynein mediates the JLP focus formation

The retrograde movement of JLP during the formation of the JLP focus in the perinuclear region suggests that the retrograde motor protein dynein is involved. To examine the role of motor proteins in the formation of JLP foci mediated by arsenite, we used erythro-9-[3-(2-hydroxynonyl)] adenine (EHNA) and rose bengal lactone (RBL) to inhibit dynein and kinesin-1, respectively (*20*) (Fig. 3A). Results show that EHNA, but not RBL, inhibited the formation of JLP foci, suggesting that JLP focus formation involves the retrograde motor dynein. The physical interaction between JLP and a component of dynein, dynactin 1 (DCTN1), was shown by reciprocal coimmunoprecipitation experiments using exogenous 9E10-JLP and FLAG-DCTN1 expressed in human embryonic kidney (HEK) 293T cells using either the 9E10 or FLAG antibody (Fig. 3B). The domain of DCTN1 involved in the interaction with JLP was mapped to the N-terminal region (1 to 880 amino acids) that contains the CAP-Gly (cytoskeleton-associated protein glycin-rich) and the first coiled-coil domains (Fig. 3C). In contrast, the structurally unrelated family member JIP-1 binds to the C-terminal region (amino acids 880 to 1278) of DCTN1, which contains the second coiled-coil domain (*21*), suggesting that JLP and JIP-1 may play different roles in the dynein-mediated transport of cargos. In addition, endogenous JLP interacted with DCTN1 in vivo in H1299 cells via coimmunoprecipitation assay, with arsenite treatment enhancing their association (Fig. 3D). Together, these results suggest that dynein is involved in the movement of JLP to induce formation of the focus.

MT array radiates from JLP focus

JLP moves along MTs to its subcellular compartments within the cell (*22*). Therefore, to examine whether MTs are involved in the formation of JLP foci, we performed immunofluorescence studies on control and arsenite-stimulated cells. Results in Fig. 4A show that, in the unstimulated cells, JLP mainly appeared as punctations in the cytoplasm, while MTs appeared as arrays surrounding the nucleus. When the cells were stimulated with arsenite, JLP foci appeared, and MTs formed arrays radiating from intense centers that overlapped with JLP foci. Some JLP punctations also overlapped with MTs. Identical changes occurred upon stimulation with transforming growth factor–β (TGFβ) and high concentrations of sodium chloride (an inducer of hypertonic stress) (Fig. 4A). The intense MT centers [MT organization centers (MTOCs)] and JLP foci colocalized on the same focal plane, as shown in the confocal *z*-stack images (fig. S2). The effects of arsenite were specific to MT because the β-actin network was not affected by arsenite stimulation (Fig. 4B). α-Tubulin is usually not found in the nuclei of unstimulated cells (*23*). In addition, results in Fig. 4C show that α-tubulin was detected in the nuclear fraction after arsenite treatment, and its levels were reduced when JLP was ablated, suggesting that JLP regulates the movement of α-tubulin to the nucleus. A trace amount of JLP was detected in the nuclear fraction of the unstimulated cells, and its level increased by the arsenite treatment, suggesting the presence of nuclear JLP in the unstimulated cells and its nuclear movement after stimulation (Figs. 4C and 6 and fig. S3).

To examine the role of MTs in the formation of JLP foci, we treated the cells with various α-tubulin inhibitors. Results in Fig. 4D

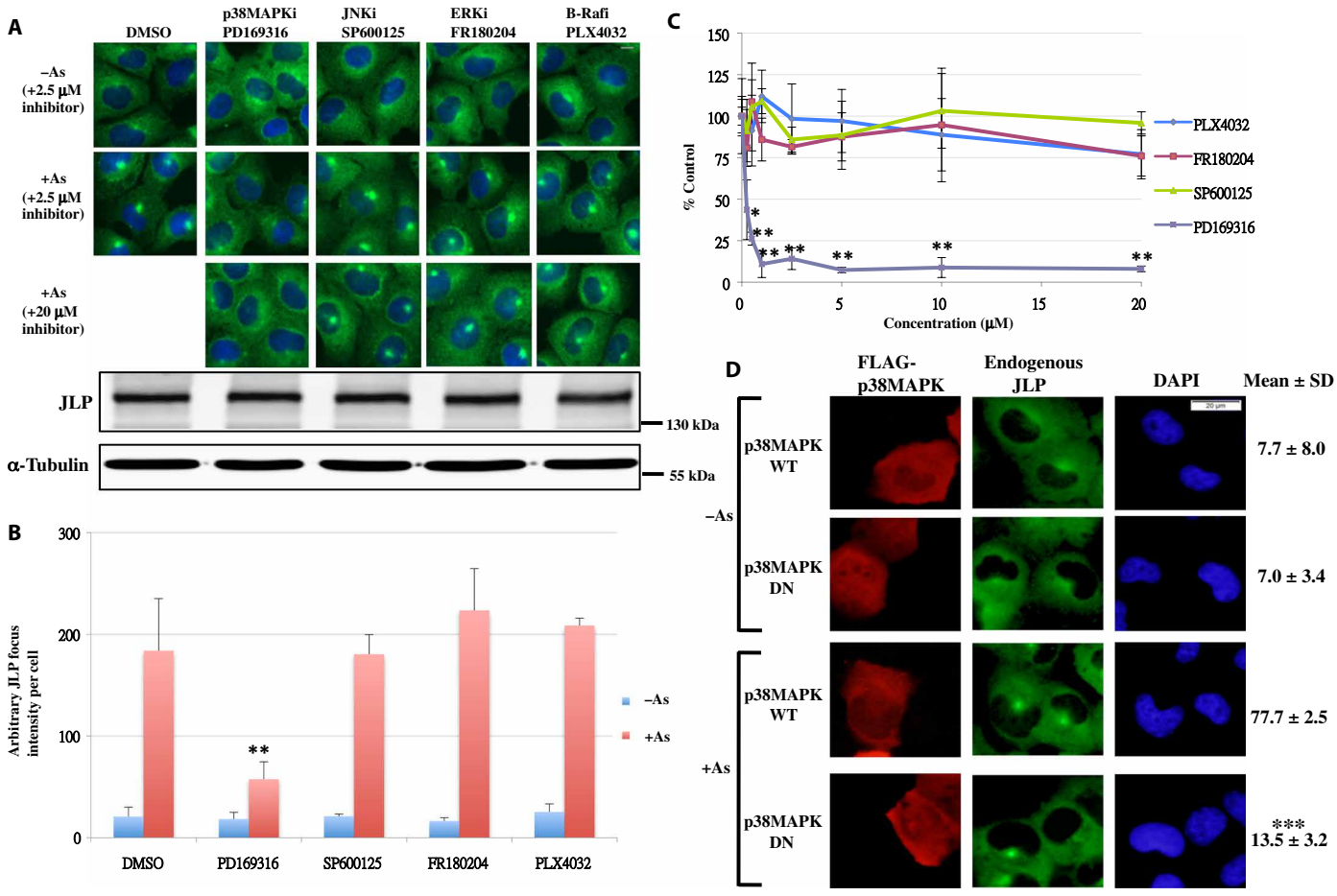

Fig. 2. p38MAPK regulates the formation of JLP focus. (**A**) Effects of kinase inhibitors (2.5 and 20 μM) on the arsenite-induced JLP focus formation. Scale bar, 10 μm. Bottom panel shows the Western blot analysis of the JLP and α-tubulin levels in those treated cells. (**B**) Quantification of the average arbitrary JLP focus intensity per cell using ImageJ in (A) at 2 μM of the inhibitors. Error bars represent SD ($n = 3$). $^{**}P < 0.02$ (as compared with the arsenite-treated vehicle control). DMSO, dimethyl sulfoxide. (**C**) Concentration effects of the kinase inhibitors. The average arbitrary JLP focus intensity per cell was calculated as percentages of their vehicle-treated controls. Error bars represent SD ($n = 4$). $^{*}P < 0.04$ and $^{**}P < 0.005$ (as compared with the corresponding untreated control). (**D**) Effects of the wild-type (WT) or dominant-negative (DN) mutant of FLAG-p38MAPK on the JLP focus formation. The percentages of cells showing the JLP foci were scored and presented as mean ± SD % ($n = 4$). $^{***}P < 0.0001$ (as compared with stimulated p38MAPK wild type–expressing cells). Scale bar, 20 μm.

show that the tubulin depolymerization inhibitor Taxol and the tubulin polymerization inhibitors vinblastine, nocodazole, and colchicine abolished the intense MT centers and caused JLP focus diffusion. Together, the results suggest that MTs control the formation of the JLP foci.

To examine the role of JLP in the formation of the radiating MT arrays, we expressed the wild-type FLAG-JLP or the dominant-negative ΔCLD mutant of FLAG-JLP in cells followed by treatment with arsenite (detailed effects of the ΔCLD mutant could be found in Fig. 5, and figs. S5 to S8). Results in Fig. 4E show that wild-type JLP allowed the formation of the radiating MT arrays, while the ΔCLD mutant inhibited array formation, showing that JLP regulates the formation of the radiating MT arrays. Together with the results in Fig. 4D, we conclude that the formation of the JLP foci and radiating MT arrays is interdependent.

MT and nuclear membrane

To determine the spatial relationship between MTs and the nuclear envelope, we treated the cells with arsenite and determined the subcellular distribution of MTs and lamin A/C, which is a component of the lamina, a filamentous meshwork underneath the inner nuclear membrane (*24*). Lamin A/C helped us define the boundary of the nucleus. Results show that in the untreated cells, the MT network was disorganized while surrounding the nucleus (Fig. 4F and figs. S4 and S9). However, in arsenite-treated cells, the MT array was formed and the MTOC pressed against the nuclear membrane deep into the nucleus. Furthermore, some MTs radiating from MTOC also depressed the nuclear membrane notably, forming some troughs. In all cases, the MTs remained outside the nucleus (Figs. 4F and 5I and figs. S4 and S9). These results suggest that the MTOC (JLP focus) physically adheres to the nuclear membrane and results in a change in the shape of the nucleus.

JLP focus contains centrosome

Since the organization of the intense MTOCs with radiating MTs closely resembled that of the mitotic asters, we probed for those components of the centrosome using immunofluorescence studies. Results show that pericentrin and γ-tubulin, the components of PCM

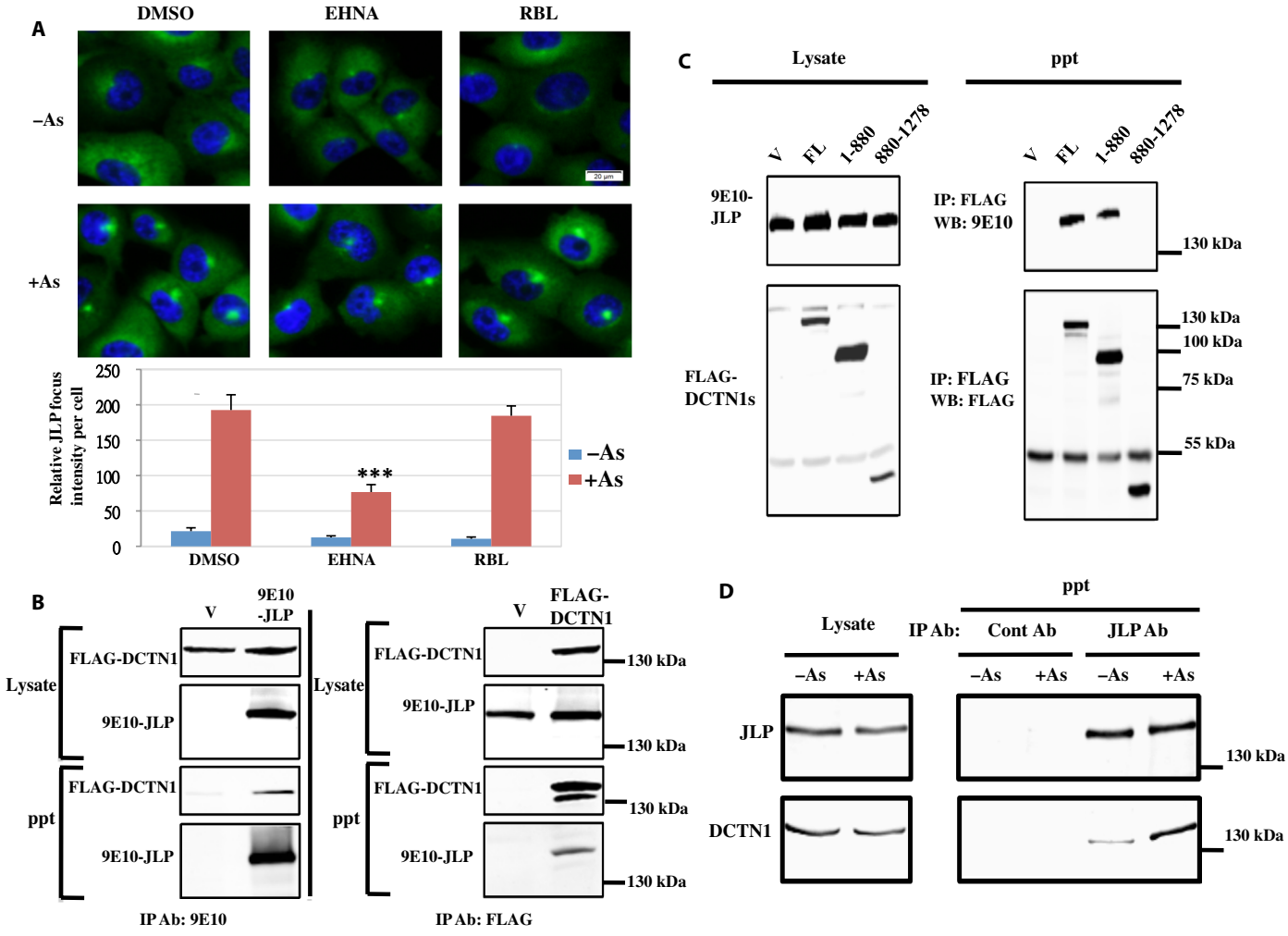

Fig. 3. Dynein regulates the retrograde movement of JLP in its focus formation. (**A**) Effects of dynein inhibitor (EHNA; 1 mM) or kinesin-1 inhibitor (RBL; 40 μM) on the JLP focus formation. The relative arbitrary JLP focus intensity per cell was calculated as in Fig. 2B. Error bars represent SD ($n = 4$). ***$P < 0.0001$ (as compared with arsenite-treated vehicle control). Scale bar, 20 μm. (**B**) Association between exogenous JLP and DCTN1. (**C**) Mapping of the domain of DCTN1 involved in association with JLP. WB, Western blotting. (**D**) Association between endogenous JLP and DCTN1 in cells treated with or without arsenite (0.5 mM) for 30 min. IP, immunoprecipitation; ppt, precipitate.

(*12*), were detected in the JLP foci (fig. S5, A and B). Furthermore, results show that the wild-type JLP coimmunoprecipitated with pericentrin in arsenite, but not vehicle-stimulated cells, suggesting that JLP interacts with centrosomes only in stimulated cells (fig. S5C). Together, these results indicate that after stimulation, JLP becomes a structural component of the PCM complex and uses centrosomes to nucleate the radiating arrays of MTs.

The JLP CLD

The JLP focus acts as a structural component of a centrosome, suggesting that a domain of JLP binds to the centrosome. To map the centrosome localization domain (CLD), we expressed wild-type and various hemagglutinin (HA)–tagged deletion and domain mutants of JLP (fig. S5D) and treated the transfected cells with arsenite followed by immunofluorescence studies. Results in fig. S5E show that wild-type JLP and the Domain C deletion mutant (JLPΔ1) could bind the centrosome and form a focus. However, further deletion of amino acids 395 to 1002 abolished the centrosome binding activity (JLPΔ2). Furthermore, the Domain III (amino acids 464 to 1002) mutant could bind centrosomes, while the other domain mutants could not, suggesting that the Domain III of JLP contains the CLD. To refine the mapping of CLD, we created a mutant (FLAG-JLPΔCLD) with the deletion of amino acids 555 to 585 (fig. S5D). The deletion of these sequences abolished 85% of the centrosome-binding activity (fig. S5F). Therefore, the amino acids 555 to 585 were defined as the CLD. To further demonstrate that the sequence is a functioning CLD, we created a missense K580N and R582Q double mutant (FLAG-JLPmutCLD), which inhibited 32% of its ability to bind to the centrosome (fig. S5, D and F). To determine whether the CLD could bind centrosome by itself, we expressed the enhanced green fluorescent protein–tagged CLD (amino acids 555 to 585) and the Domain III in cells. The Domain III, but not the CLD, could bind centrosomes after the arsenite treatment, showing that CLD of JLP is necessary, but not sufficient, to interact with centrosomes (fig. S6).

To demonstrate the role of CLD in JLP focus formation, we expressed the FLAG-tagged wild-type JLP, as well as its mutants (JLPΔCLD and JLPmutCLD) and found that they inhibited the ability of JLP to form foci by 92 and 52%, respectively (fig. S7A). As JLP is

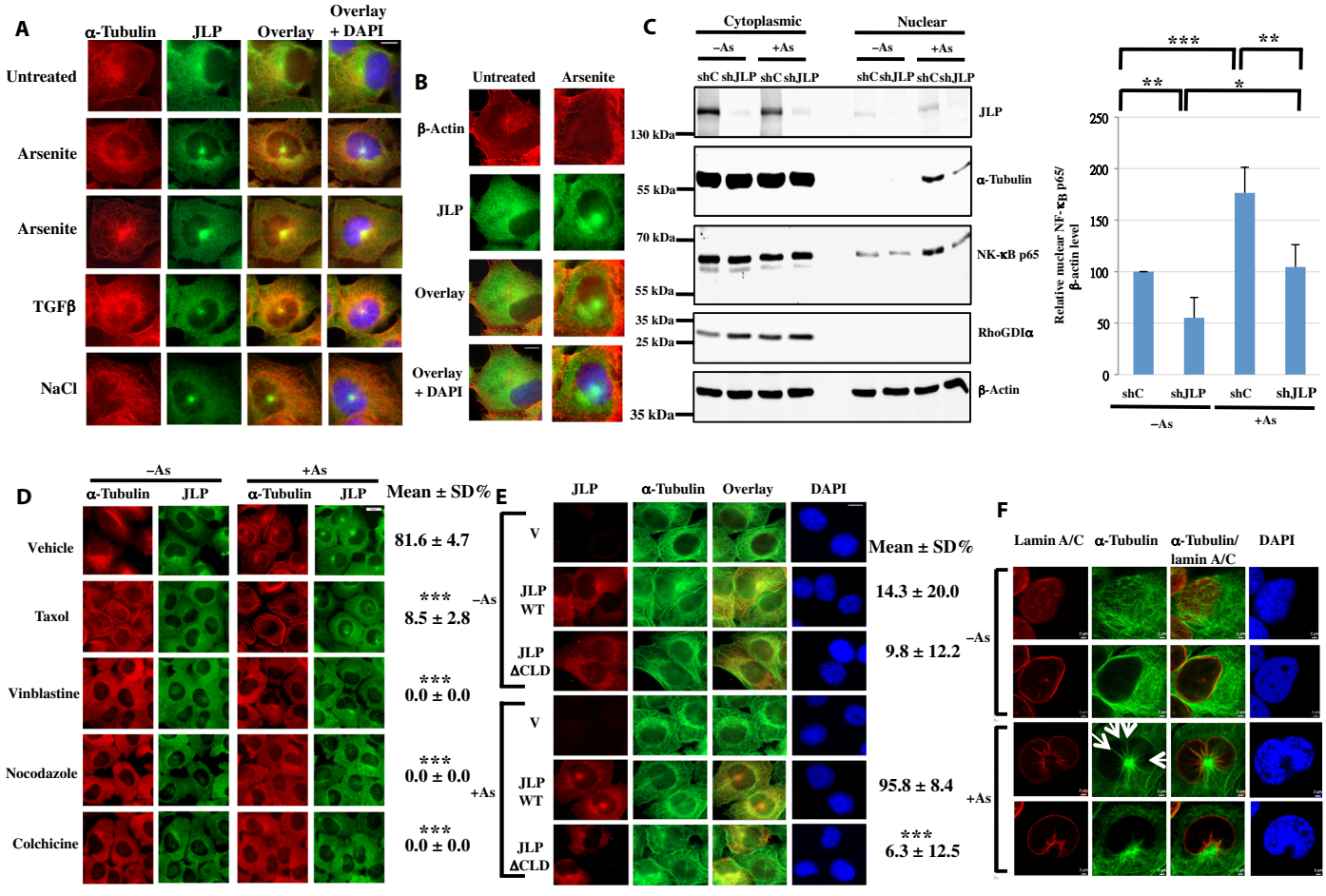

Fig. 4. Formation of JLP focus and MT array is interdependent. (**A**) Induction of JLP foci and MT arrays by arsenite (0.5 mM), NaCl (500 mM), or TGFβ (5 ng/ml) for 30 min. Scale bar, 10 μm. (**B**) Arsenite does not affect the β-actin network. H1299 cells were treated with or without arsenite (0.5 mM) for 30 min. Scale bar, 10 μm. (**C**) Influx of α-tubulin to the nucleus induced by arsenite and its dependence on JLP. shC and shJLP denote the control and JLP-ablated cells, respectively. Ablation of JLP also reduces the nuclear translocation of NF-κB p65. RhoGDIα is a marker for the cytoplasmic fraction. The relative nuclear NF-κB p65 levels are quantified and presented as mean ± SD ($n = 4$). *$P < 0.02$, **$P < 0.005$, and ***$P < 0.001$. (**D**) MT-modulating agents inhibit the formation of JLP foci. The percentages of cells showing the JLP foci and the MT arrays were scored and presented as mean ± SD % ($n = 4$). ***$P < 0.0001$ (as compared with arsenite-treated control cells). Scale bar, 20 μm. (**E**) ΔCLD mutant of JLP inhibits the formation of the MT arrays. The percentages of cells showing the JLP foci and the MT arrays were scored and presented as mean ± SD % ($n = 4$). ***$P < 0.0001$ (as compared with arsenite-treated FLAG-JLP wild-type cells). Scale bar, 10 μm. (**F**) The top surface and medial views of lamin A/C and MTs in cells treated with or without arsenite (0.5 mM) for 40 min. The radiating MTs creating troughs on the nuclear membrane are indicated by arrows. Scale bars, 2 μm. Confocal *z*-stack images are shown in fig. S4.

known to form homodimers (*17*), these CLD mutants acted as dominant-negative mutants by forming dimers with wild-type JLP and inhibiting the formation of JLP foci (fig. S7B).

The CLD of JLP is not conserved among the JIP family members. Therefore, the formation of focus is potentially unique to JLP. Results in fig. S7 (C and D) show that JLP, but not JIP-1, JIP-2, and JIP-3, formed foci after arsenite stimulation, suggesting that the CLD sequence of JLP is unique and necessary for the formation of the foci. Within the CLD, there is a putative nuclear localization signal, which contains a bipartite signal sequence (two clusters of basic amino acids separated by a spacer: 555NTT**KK**PEPPVN-LKYNAPTSHVTPSV**KKR**SST585). When missense mutations were introduced to K580 and R582, the resulted double mutant (JLPmutCLD) exhibited a reduced ability to bind centrosomes and form foci (figs. S5F and S7A), suggesting that the CLD is important for the focus functions.

JLP focus contains PLK1

Centrosomes form MT arrays in mitosis when they are primed for maturation and nucleation of MTs by kinases such as PLK1 (*25*). For a fair comparison of cells in the same cell cycle phase, we subjected cells to a double thymidine block before their release and subsequent treatment with various stimuli. The cells were probed for the expression of cyclin B2, which is a marker for cells in the G_2 and M phases of the cell cycle (*26*). In addition, we examined both unstimulated and stimulated cells that were in the G_2 phase (high cyclin B2 expression and intact nuclear morphology). Under these experimental conditions, we showed in fig. S8A that two intense spots of PLK1 colocalized with the JLP focus after stimulation with not only arsenite but also with TGFβ and tumor necrosis factor–α (TNFα).

To show the effects of the JLPΔCLD mutant, we subjected the cells expressing FLAG-tagged wild-type and ΔCLD mutant of JLP

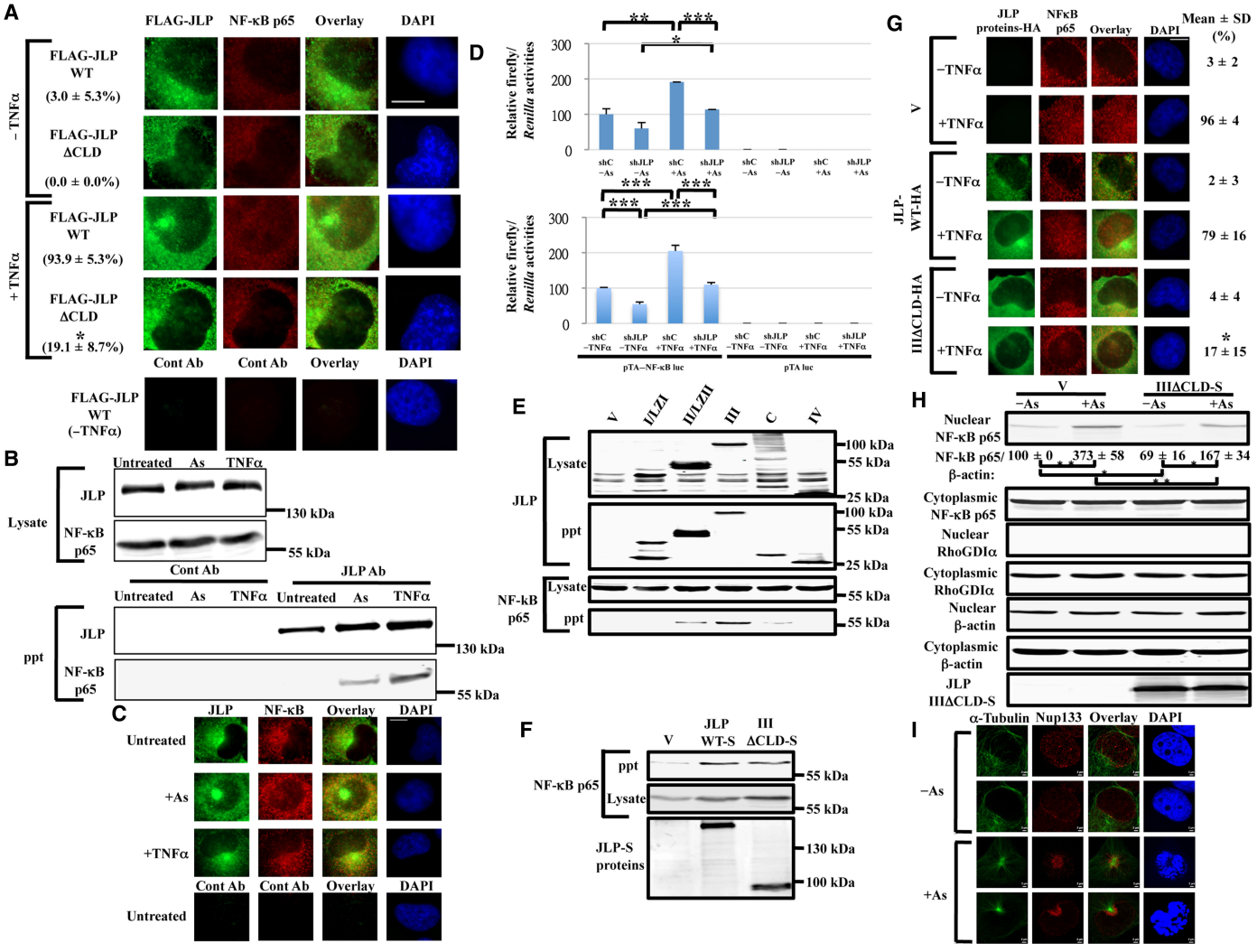

Fig. 5. Stimulated nuclear translocation of the endogenous NF-κB p65 depends on the JLP focus. (**A**) The JLPΔCLD mutant inhibits the nuclear translocation of NF-κB p65 in H1299 cells. The percentages of cells showing the nuclear NF-κB p65 were scored and presented as mean ± SD % ($n = 3$). *$P < 0.0003$ (as compared with arsenite-treated FLAG-JLP wild-type cells). (**B**) Interaction between endogenous JLP and NF-κB p65. HEK293T cells were serum-deprived for 16 hours before they were stimulated with arsenite (0.5 mM) or tumor necrosis factor–α (TNFα; 30 ng/ml) for 25 min. The cell lysates were precipitated with the JLP antibody. (**C**) Colocalization of JLP and NF-κB p65. H1299 cells were stimulated with arsenite (0.5 mM) or TNFα (30 ng/ml) for 10 min before they were stained for immunofluorescence studies. Puncta of the colocalized JLP–NF-κB p65 appear orange. (**D**) Ablation of JLP reduces the transactivation of NF-κB in H1299 cells stimulated with arsenite (top) or TNFα (bottom). shC and shJLP denote the control and JLP-ablated cells, respectively. The relative NF-κB transactivation activities are presented as mean ± SD ($n = 3$). *$P < 0.02$, **$P < 0.01$, and ***$P < 0.005$. (**E**) Association of the S-tagged JLP domains with NF-κB p65 after arsenite stimulation (0.5 mM for 45 min). (**F**) Binding of the S-tagged Domain IIIΔCLD with NF-κB p65 after arsenite stimulation (0.5 mM for 45 min). (**G**) Reduction of NF-κB p65 nuclear translocation by IIIΔCLD in immunofluorescence studies in H1299 cells treated with or without TNFα (10 ng/ml) for 25 min. The percentages of cells showing the nuclear NF-κB p65 were scored and presented as mean ± SD % ($n = 3$). *$P < 0.002$ (as compared with the treated V cells). (**H**) Reduction of NF-κB p65 nuclear translocation by IIIΔCLD in subcellular fractionation studies in COS-7 cells. Transiently transfected COS-7 cells were stimulated with or without arsenite (0.5 mM) for 45 min, followed by fractionation. The relative nuclear NF-κB p65/β-actin levels are quantified and presented as mean ± SD ($n = 4$). *$P < 0.01$ and **$P < 0.001$. Scale bar, 10 μm. RhoGDIα is a marker for the cytoplasmic fraction. (**I**) Top surface and medial views of Nup133 and MTs on the nuclear membrane in the cells treated with or without arsenite (0.5 mM) for 40 min. Scale bars, 2 μm.

to the identical experimental conditions as described above and observed that that two intense spots of PLK1 were present in the JLP foci in the wild-type FLAG-JLP–expressing cells in response to arsenite, TGFβ, and TNFα (fig. S8B). However, no such intense spots of PLK1 were formed in the ΔCLD mutant expressing cells, suggesting that JLP tethers PLK1 to the focus. This result is expected as JLP has been shown to interact with PLK1 in a specific manner (*27*). In addition, we preincubated cells with the pan-PLK inhibitor BI2536 (*27*) or the casein kinase 2 inhibitor CX4945 as a negative control before stimulating cells with arsenite. Results in fig. S8C show that JLP foci were formed and PLK1 colocalized with the foci in response to all treatments; however, the MT array formation was inhibited by the PLK1 inhibitor only, suggesting that PLK1 kinase activity is not required in the formation of JLP foci but is involved in the nucleation of MT arrays induced by extracellular signals.

JLP interacts with the Polo-box domain (PBD), but not the Polo-kinase domain (PKD) of PLK1 in HEK293T cells (*27*). To examine whether JLP directly interacts with PLK1, we performed

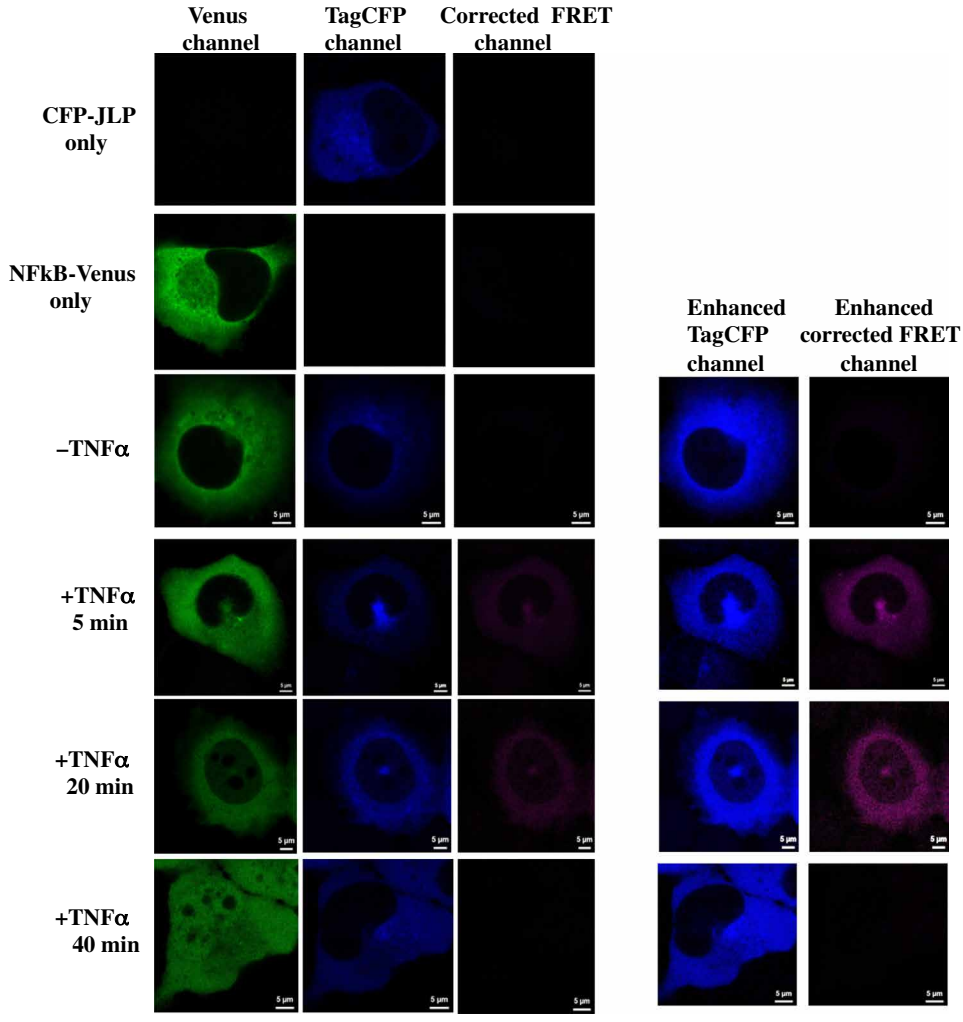

Fig. 6. FRET confocal microscopy of JLP and NF-κB p65. TagCFP-JLP and NF-κB p65-Venus (NF-κB–Venus) were expressed in H1299 cells. They were treated with or without TNFα (10 ng/ml) for the indicated period of time. Confocal images were taken and analyzed for FRET. The FRET signals were corrected for the bleed-through signals. Some images were enhanced to show the trace amount of JLP and FRET signals in the nucleus 20 min after stimulation. Scale bars, 5 μm.

an in vitro glutathione *S*-transferase (GST) pull-down assays using bacterial recombinant S-tagged JLP and GST-PLK1 proteins (wild-type, PKD, and PBD). The results in fig. S8D show that GST-PBD could not pull down JLP, suggesting that JLP and PLK1 do not interact directly. However, we do not exclude the possibility of their direct interaction when they are posttranslationally modified.

JLP focus controls NF-κB translocation

The formation of JLP foci and radiating MT arrays that extend to the nucleus suggests that cellular factors in the cytoplasm can be transported to the nucleus along the arrays in a JLP- and MT-dependent manner. We therefore examined the subcellular localization of NF-κB p65, a transcription factor kept latent in the cytoplasm and transported to the nucleus upon activation by stress stimuli or proinflammatory cytokines (*13*) in the context of JLP expression and MTs, which have been shown to associate with NF-κB and modulates its activation (*15*). To test whether the transport of NF-κB p65 is JLP dependent, we expressed the wild-type and ΔCLD mutant of JLP in cells, followed by stimulation with the proinflammatory cytokine TNFα and subsequent immunofluorescence studies. Results in Fig. 5A show that there were a few NF-κB p65 puncta inside the nucleus before TNFα stimulation. However, after TNFα stimulation, the wild-type JLP formed foci, and a large number of NF-κB p65 puncta could be detected in the nucleus. Furthermore, JLPΔCLD mutant expression impaired both the JLP focus formation and the entrance of NF-κB p65 into the nucleus, indicating that JLP is important for the transport of NF-κB p65 to the nucleus. Furthermore, ablation of JLP reduced the levels of NF-κB p65 transported to the nucleus (Fig. 4C).

We next performed immunoprecipitation assays to demonstrate the interaction between JLP and NF-κB p65. Figure 5B shows that NF-κB p65 interacted with JLP after stimulation with arsenite or TNFα. Furthermore, there were a few colocalized JLP–NF-κB p65 puncta in the cytoplasm before stimulation with these agents. After stimulation, there was an appearance of some colocalized JLP–NF-κB p65 puncta in the nucleus and many puncta in the cytoplasm, especially in the perinuclear region (Fig. 5C). The interaction between JLP and NF-κB p65 was substantiated by fluorescence resonance

energy transfer (FRET) confocal microscopy (Fig. 6) (*28*). FRET occurs between two fluorophores only when they are in close proximity and correct orientation. TagCFP (Tag cyan fluorescent protein)–tagged JLP (TagCFP-JLP) and Venus-tagged NF-κB p65 (NF-κB–Venus) were expressed in H1299 cells. Cells were treated TNFα for different periods of time, where the single-protein controls showed signals in their appropriate channels, but not in the FRET channel (Fig. 6). When both proteins were expressed, they did not exhibit FRET signals in the unstimulated cells, suggesting that JLP and NF-κB p65 do not interact without stimulation. However, 5 min after stimulation, the cells showed the FRET signals in the cytoplasm, suggesting that JLP and NF-κB p65 interact shortly after stimulation. These results are consistent with the results in Fig. 5 (B and C). Furthermore, in addition to the FRET signals in the cytoplasm, NF-κB p65 as well as a trace amount of FRET and JLP signals were detected in the nucleus 20 min after stimulation, showing that JLP and NF-κB p65 move together into the nucleus. However, 40 min after stimulation, NF-κB p65 remained in the nucleus, while the JLP level in the nucleus and the overall FRET signals were reduced, suggesting that NF-κB p65 is dissociated from JLP and unloaded in the nucleus.

To examine whether JLP is involved in the transactivation of NF-κB p65 mediated by arsenite, we performed luciferase assays using a luciferase reporter containing the NF-κB–responsive element in cells expressing a scramble short hairpin RNA (shRNA) (shC) or a JLP-specific shRNA (shJLP). Figure 5D shows that there was basal NF-κB transactivation activity in the control cells, which were reduced in the JLP-ablated cells. When the cells were treated with arsenite, NF-κB transactivation activity was increased in the control cells but reduced in JLP-ablated cells, suggesting that JLP is involved in the NF-κB transactivation. These results further support the notion that JLP is involved in transporting NF-κB to the nucleus to transactivate gene expression. Similar results were also obtained with TNFα (Fig. 5D, bottom).

To identify the JLP domain involved in binding NF-κB p65, we conducted pull-down assays using S-tagged JLP domains. Results show that the Domains II/LZII, III, and C bound NF-κB p65 and the Domain III, exhibiting the highest affinity for NF-κB p65 (Fig. 5E).

Because the Domain III contains the CLD, which is involved in binding the centrosome and the formation of the MT array upon stimulation, we generated a CLD deletion mutant of Domain III (IIIΔCLD). Results show that IIIΔCLD bound NF-κB p65 (Fig. 5F), but not the centrosome (fig. S5E), suggesting that the Domain III, and not the CLD, is involved in binding NF-κB p65. Furthermore, we used this mutant for competition in immunofluorescence and subcellular fractionation assays. Results show that, upon extracellular stimulation, IIIΔCLD reduced the nuclear translocation of NF-κB p65 (Fig. 5, G and H), suggesting that the association between JLP and NF-κB p65 is important for the nuclear translocation of NF-κB p65 mediated by extracellular stimulation.

To determine whether the MTOC (JLP focus) is involved in the unloading of NF-κB p65 to the nucleus through the nuclear pores, we probed for the component of the nuclear pore Nup133 (*29*) and MTs in cells treated with or without arsenite. In the untreated cells, the nuclear pores were randomly disturbed on the nuclear membrane (Fig. 5I). After stimulation with arsenite, numerous nuclear pores were concentrated at the contact surface of the nuclear membrane with the MTOC (JLP focus), suggesting that the close contact of the MTOC (JLP focus) to the nuclear membrane attracts the nuclear pores, and the cargos (NF-κB p65) traveling along MTs can easily be unloaded through the nuclear pores at the contact membrane surface with the JLP focus. Similar results were obtained with another nuclear pore component, Nup358 (*30*), by confocal microscopy (fig. S9A) and high-resolution stimulated emission depletion (STED) microscopy (fig. S9B).

DISCUSSION

When cells are stimulated, p38MAPK becomes activated and triggers the dynein-dependent transport of a large amount of JLP to the centrosome for JLP focus formation. JLP engages the centrosome and PLK1, leading to centrosome maturation and nucleation of MT array. Mature centrosomes are known to form bipolar mitotic and meiotic spindles (arrays of MTs) that are involved in segregating the chromatids (*25*). Here, monopolar spindles are formed for the transport of cellular factors to the nucleus in cells stimulated by extracellular stimuli (fig. S10). The interdependence of the formation of the JLP focus and the radiating MT array (Fig. 4, D and E) suggests that both are essential to establish each other. At the molecular level, this may be due to the fact that JLP is an essential structural component for the mature centrosomes, and that the MT array is essential for JLP to move to and interact with centrosomes for focus formation.

There are differences in the formation of the mitotic asters and in that induced by extracellular stimuli. First, mitotic aster formation is cell cycle dependent and occurs in metaphase, while the formation of the induced aster is inducible by extracellular stimuli and occurs in the interphase cells. Second, there is a duplication of centrosomes before the formation of the mitotic asters (bipolar spindles) (*25*), while the formation of the induced aster does not require the duplication (monopolar spindle). Third, the spindles of mitotic asters are formed in all directions, while the directions of spindle formation for the induced aster are restricted by the nuclear membrane. All of these differences suggest that the mechanisms governing their formation may not be identical.

JLP is ubiquitously expressed in many cell types, while the other JIP family members are cell type specific (*2*, *17*), suggesting that JLP serves common purposes in those cell types. In the present study, many cell types form JLP foci upon arsenite stimulation. Diverse extracellular stimuli also induce the formation of JLP focus–MT array, suggesting that the JLP-mediated transport network is commonly engaged for intracellular transport of cellular factors to different subcellular compartments. Together, the studies define new roles for JLP and the centrosome/MT in intracellular transport and signal transduction induced by extracellular stimuli.

The studies also provide a mechanism for the p38MAPK-dependent activation and nuclear translocation of NF-κB observed by others (*31*), in which p38MAPK serves as a kinase that initiates the formation of the transport network for the nuclear translocation of NF-κB. Furthermore, various stress stimuli and proinflammatory cytokines activate p38MAPK activity (*32*). It becomes important that those stimuli rely on p38MAPK as the same triggering mechanism to initiate the formation of the JLP-mediated transport system to facilitate the transport of various signaling molecules to the nucleus (*31*).

Previously, NF-κB, as well as other proteins, is transported by dynein along MTs to the perinuclear region (*16*, *33*). The present studies show that, upon stimulation with various extracellular stimuli, p38MAPK is activated, which, in turn, stimulates the retrograde movement of dynein. The JLP-centrosomes-MTarray also establishes a transport network from the cytoplasm toward the nuclear surface. Furthermore, the MTOC (JLP focus) forms a tight physical adherence

to the nuclear membrane and concentrates numerous nuclear pores at its contact surface to facilitate the transport of NF-κB along MTs to the nucleus (fig. S10). This also shows that the nuclear pores are dynamic structures that response to extracellular stimuli. Two hypotheses of unloading NF-κB are proposed: The NF-κB–JLP-dynein complexes move along the MT into the nucleus to unload NF-κB. Alternatively, the NF-κB–JLP-dynein complexes move to the nuclear membrane and unload NF-κB–JLP through nuclear pores into the nucleus. Further experiments are needed to differentiate between the hypotheses (fig. S10).

It is very likely that JLP serves as a scaffolding protein to tether NF-κB and dynein. Such complex moves along MT to unload NF-κB to the nucleus. Furthermore, JLP also tethers PLK1 to the focus that contains a centrosome. Therefore, JLP may also serve as a scaffolding protein to tether PLK1 to the centrosome for its maturation and nucleation of MT array. In this case, JLP serves as a structural component of the mature centrosome. In addition, another PLK family member, PLK3, which is active in the interphase and activated by stress stimulus, may also participate in the process (*34*).

JLP, also known as SPAG9, is a biomarker for various cancer types including renal, breast, thyroid, cervical, lung, colon, and hepatocellular carcinomas as well as astrocytoma (*35*). JLP levels are elevated in those cancer types compared with their normal controls. In addition, JLP contributes to malignancy by promoting cellular proliferation, migration, and colony formation (*36*, *37*). JLP has been shown to correlate with poor prognosis of patients with cancer (*35*). Similarly, p38MAPK is also involved in processes, such as proliferation, differentiation, migration, and invasion. Deregulation of p38MAPK levels in patients are associated with advanced stages and short survival in patients with cancer (*38*). Their functional similarities suggest that JLP and p38MAPK may confer malignancy by acting synergistically to transport proteins, like NF-κB, involved in cancer malignancy between the cytoplasm and nucleus. Therefore, targeting or ablating JLP and p38MAPK may have therapeutic advantages to treat those cancers (*39*). Furthermore, targeting dynein, which is involved in the transport of NF-κB, may also be of therapeutic value.

The identification of the nuclear localization signal explains the presence of the nuclear form of JLP and the ability of JLP to bind diverse proteins in the cytoplasm and nucleus. It is possible that JLP shuttles between the two subcellular compartments, which is highly likely considering that JLP associates with the anterograde and retrograde motor proteins that move in opposite directions along MTs (*5*, *8*, *9*, *22*). Here, we describe extracellular stimuli–driven retrograde movements of JLP to transport NF-κB p65 to the nucleus, where it is unloaded (Figs. 4C and 6). To our knowledge, it is the first report of a scaffolding protein binding and translocating cargo into the nucleus.

In conclusion, JLP exhibits multiple functions in the nuclear translocation of NF-κB p65: (i) It tethers PLK1 to the centrosome for its maturation, leading to the formation of a JLP focus and the MT array. (ii) It transports NF-κB p65 along MTs to the nucleus. (iii) The JLP focus depresses the nuclear membrane and concentrates the nuclear pores at its contact surface. (iv) It complexes with NF-κB p65 into the nucleus for its unloading.

MATERIALS AND METHODS

Materials

The following reagents were obtained commercially: anti-HA antibodies [sc-7392, sc-805 (Santa Cruz Biotechnology)], anti-RhoGDIα [sc-7392 (Santa Cruz Biotechnology)], anti-DCTN1 antibody [sc-365274 (Santa Cruz Biotechnology)], anti-Mad1 antibody [sc-222 (Santa Cruz Biotechnology)], anti-FLAG antibody [sc-807 (Santa Cruz Biotechnology)], anti-9E10 antibody [sc-40 (Santa Cruz Biotechnology)], anti–S-tag antibody [sc-802 (Santa Cruz Biotechnology)], anti–NF-κB p65 antibodies [8242 (Cell Signaling Technology), sc-8008 (Santa Cruz Biotechnology), and 10745-1-AP (Proteintech)], anti–cyclin B2 antibody [sc-5233 (Santa Cruz Biotechnology)], anti-GST antibody [sc-138 (Santa Cruz Biotechnology)], anti-PLK1 antibody [sc-17783 (Santa Cruz Biotechnology)], anti-Nup133 [sc-376763 (Santa Cruz Biotechnology)], anti-Nup358 (Ran BP-2) [sc-74518 (Santa Cruz Biotechnology)], anti–lamin A/C [sc-376248 (Santa Cruz Biotechnology)], anti–β-actin antibody [A2228 (Sigma-Aldrich)], anti–α-tubulin [A4026 (Sigma-Aldrich)], fluorescein isothiocyanate (FITC)–conjugated anti–α-tubulin [F2168 (Sigma-Aldrich)], anti–γ-tubulin [A6557 (Sigma-Aldrich)], anti-pericentrin [ab4448 (Abcam)], pTagCFP-C (Evrogen), ptdTomato (Clontech), EHNA [E114 (Sigma-Aldrich)], Texas Red–conjugated phalloidin for β-actin [T7471 (Life Technologies)], RBL [328960 (Sigma-Aldrich)], arsenite [714216 (Thermo Fisher Scientific)], Taxol [T1912 (Sigma-Aldrich)], vinblastine [V1337 (Sigma-Aldrich)], nocodazole [M1404 (Sigma-Aldrich)], colchicines [C3915 (Sigma-Aldrich)], BI2536 [S1109 (Selleckchem)], CX4945 [S2248 (Selleckchem)], p38MAPK inhibitor PD169316 [P9248 (Sigma-Aldrich)], JNK inhibitor SP600125 [420119 (Calbiochem)], ERK inhibitor FR180204 [328007 (Calbiochem)], B-Raf inhibitor PLX4032 [A-1130 (Active Biochem)], S-protein agarose [69704 (Novagen)], glutathione agarose [G4510 (Sigma-Aldrich)], Protein A Sepharose CL-4B [17-0780-01 (GE Healthcare)], TNFα [cyt-223B [ProSpec-Tany TechnoGene)], and TGFβ1 [240-b (R&D Systems)]. The JLP antibody was a rabbit polyclonal antibody raised against the C terminus of the mouse JLP (amino acids 793 to 1307) and cross-reacted with the human JLP. The IL-17 receptor (IL-17R) rabbit polyclonal antibody was raised against amino acids 656 to 864 of the mouse IL-17R and cross-reacted with the human IL-17R. The details of the domain structure of JLP and its domain mutants have been described previously (*1*).

shRNAs and small interfering RNAs

The target sequences of the shRNA against JLP (shJLP) and the control scramble shRNA (shC) were 5′-ATTCTAAAGATTCCACTCGGG-3′ and 5′-CCTAAGGTTAAGTCGCCCTCGCTC-3′, respectively. Their clone numbers were TRCN0000148831 (Dharmacon) and plasmid 1864 (Addgene), respectively. The target sequences of the small interfering RNA (siRNA) against JLP (siJLP) and the control siRNA (siC) were the same as those of shJLP and shC, respectively. The double-stranded siRNAs were synthesized by Dharmacon.

Cell culture

HEK293T, COS-7, SHSY-5Y, and H1299 cells were grown in Dulbecco's modified Eagle's medium supplemented with 10% fetal bovine serum. Cell cultures were maintained at 37°C with 5% CO_2.

Transient transfection

For plasmid transfection, cells were transfected using Lipofectamine 2000 (Invitrogen) or X-tremeGENE 9 (Roche) according to the manufacturers' instructions. The plasmid/transfection reagent complex was formed in Opti-MEM (Invitrogen), and then added to cells. After transfection, the cells were replenished with growth medium.

Subcellular fractionation

Cytoplasmic and nuclear fractions were prepared as described (*40*). Briefly, cells were suspended in 400 μl of hypotonic buffer 1 [10 mM Hepes-KOH (pH 7.9), 10 mM KCl, 0.1 mM EDTA, 0.1 mM EGTA, and 1 mM dithiothreitol (DTT) together with protease and phosphatase inhibitors] by gentle pipetting, and the suspension was incubated on ice for 15 min. To this suspension, 25 μl of 10% Nonidet P-40 (NP-40) was added, vortexed for 10 s, and centrifuged at 1300*g*. The supernatant constituted the cytoplasmic extract, while the nuclear pellet was further washed in 500 μl of hypotonic buffer once and finally lysed in buffer C with 0.2% NP-40 [20 mM Hepes-KOH (pH 7.9), 400 mM NaCl, 0.2% NP-40, 1 mM EDTA, 1 mM EGTA, and 1 mM DTT together with protease and phosphatase inhibitors] on ice for 20 min. The lysate was spun, and the supernatant constituted the nuclear fraction. RhoGDIα is a cytoplasmic protein and serves as an indicator of the nuclear fraction purity.

Western blot analysis

The cell lysates or immunoprecipitates were resolved by SDS–polyacrylamide gel electrophoresis. The resolved proteins were transferred onto nitrocellulose membranes, which were blocked in Blocking Buffer for Fluorescent Western Blotting (Rockland). Appropriate primary antibodies were added to the membranes in the blocking buffer containing 0.1% Tween-20 at 4°C overnight. Membranes were washed three times with washing buffer [phosphate-buffered saline (PBS)/0.1% Tween 20] before they were incubated with IRDye 680RD– and IRDye 800CW–conjugated secondary antibodies (Odyssey) at room temperature for an hour. The membranes were washed three times with the washing buffer, and the immunoreactive protein bands were detected by the Odyssey Infrared Imaging System.

Fluorescence microscopy

The cells were fixed with 4% paraformaldehyde for 30 min and permeabilized in 0.1% Triton X-100 in PBS for 30 min. These studies were conducted similarly as described using specific antibodies as indicated (*20*). Alexa Fluor 488– and/or Alexa Fluor 568–conjugated secondary antibodies (Invitrogen) were used. The nuclei were stained with the DNA-intercalating dye 4′,6-diamidino-2-phenylindole. The cells were analyzed under a fluorescence microscope (Olympus IX71 FluoView). Images were captured using the DP72 Olympus camera system and cellSens software. Alternatively, images were captured using Zeiss Axio Imager.A2 (white field) or Zeiss LSM 880 Airyscan (confocal) together with the Zen software. The average arbitrary JLP focus intensity per cell was quantitated using ImageJ. High-resolution STED images were acquired on a Leica TCS SP8 STED 3X. Cells were labeled with FITC-conjugated α-tubulin antibody and Nup358 antibody with secondary antibody Alexa Fluor 647. Images were acquired at 400 Hz with gated HyD detectors (adjusted between 0.3 and 6 ns) and a 100× oil immersion objective (Leica) with 5× zoom to obtain the desired pixel size (20 nm). Alexa Fluor 647 was excited with the 653-nm line (4 to 10%), and the pulsed 775-nm depletion line (8%) was used to generate STED. FITC was excited with the 495-nm line (1 to 4%) and the continuous-wave 594-nm depletion laser (20%) was used to generate STED. The images were analyzed by Leica Suite X.

FRET confocal microscopy

Confocal images were acquired with Zeiss LSM 880 Airyscan. Filter sets used were as follows: the TagCFP channel (donor excitation/donor emission = 458/480 nm), the Venus channel (acceptor excitation/acceptor emission = 515/528 nm), and the FRET channel (donor excitation/acceptor emission = 458/528 nm). The FRET signals were corrected for the bleed-through fluorescence.

Pull-down assays

Cells were transfected to express S-tagged proteins, followed by serum deprivation for at least 16 hours before they were lysed and sonicated in Hepes-100 buffer (*41*) supplemented with guanosine triphosphate (GTP) (1 mM), bovine serum albumin (BSA; 2 mg/ml), and protease inhibitors. The cell lysates were sonicated and spun at 1300*g* before they were precipitated with S-protein agarose beads for 2 hours. For immunoprecipitation with the JLP antibody, Protein A Sepharose CL-4B beads were added after the incubation with the antibody. The precipitates were washed with the lysis buffer twice, followed by the lysis buffer without BSA once. The precipitates and the lysates were analyzed by Western blotting. For the GST-fusion proteins, glutathione agarose beads were used; the lysis/pull-down buffer contained 50 mM Hepes (pH 7.5), 70 mM potassium acetate, 5 mM magnesium acetate, 35 mM NaCl, 0.2% Triton X-100, and protease inhibitors as described (*27*).

Luciferase assays

H1299 cells expressing a scramble shRNA (shC) or a specific shRNA against JLP (shJLP) were seeded in 24-well culture dishes and transfected with the parental firefly luciferase vector (pTA luc) or a luciferase reporter with the NF-κB–responsive element (pTA–NF-κB luc) vector (Clontech), together with the *Renilla* luciferase vector (pRL-CH110) (*42*) and an expression plasmid for NF-κB. The next day, the transfected cells were replenished with fresh medium and treated with arsenite (60 μM). Sixteen hours later, they were assayed for the firefly and *Renilla* luciferase activities using the Dual-Luciferase Reporter Assay (Promega). For the treatment of TNFα, the transfected cells were serum-deprived for 16 hours before they were treated with TNFα (30 ng/ml) for 4 hours, followed by the luciferase assays.

Statistics

Statistical analyses were performed using the unpaired *t* test by GraphPad Prism (GraphPad Software). $P < 0.05$ was considered significant.

SUPPLEMENTARY MATERIALS

Supplementary material for this article is available at http://advances.sciencemag.org/cgi/content/full/5/8/eaav0318/DC1

Fig. S1. Specificity of the JLP antibody.
Fig. S2. Colocalization of JLP focus and the MTOC.
Fig. S3. Nuclear JLP.
Fig. S4. The MTOC and nuclear membrane.
Fig. S5. The role of the CLD in the association of JLP focus with centrosome.
Fig. S6. The CLD does not bind centrosome.
Fig. S7. The role of the CLD in the formation of JLP focus.
Fig. S8. PLK1 is a part of JLP focus.
Fig. S9. JLP focus concentrates the nuclear pore protein Nup358.
Fig. S10. Models for the formation of JLP focus and its role in nuclear translocation of NF-κB p65.

REFERENCES AND NOTES

1. C. M. Lee, D. Onésime, C. D. Reddy, N. Dhanasekaran, E. P. Reddy, JLP: A scaffolding protein that tethers JNK/p38MAPK signaling modules and transcription factors. *Proc. Natl. Acad. Sci. U.S.A.* **99**, 14189–14194 (2002).
2. D. N. Dhanasekaran, K. Kashef, C. M. Lee, H. Xu, E. P. Reddy, Scaffold proteins of MAP-kinase modules. *Oncogene* **26**, 3185–3202 (2007).

3. K. Kashef, R. Radhakrishnan, C. M. Lee, E. P. Reddy, D. N. Dhanasekaran, Neoplastic transformation induced by the gep oncogenes involves the scaffold protein JNK-interacting leucine zipper protein. *Neoplasia* **13**, 358–364 (2011).
4. H. Xu, D. N. Dhanasekaran, C. M. Lee, E. P. Reddy, Regulation of neurite outgrowth by interactions between the scaffolding protein, JNK-associated leucine zipper protein, and neuronal growth-associated protein superior cervical ganglia clone 10. *J. Biol. Chem.* **285**, 3548–3553 (2010).
5. Q. Nguyen, C. M. Lee, A. Le, E. P. Reddy, JLP associates with kinesin light chain 1 through a novel leucine zipper-like domain. *J. Biol. Chem.* **280**, 30185–30191 (2005).
6. G. Takaesu, J.-S. Kang, G. U. Bae, M.-J. Yi, C. M. Lee, E. P. Reddy, R. S. Krauss, Activation of p38α/β MAPK in myogenesis via binding of the scaffold protein JLP to the cell surface protein Cdo. *J. Cell Biol.* **175**, 383–388 (2006).
7. T. Obata, G. E. Brown, M. B. Yaffe, MAP kinase pathways activated by stress: The p38 MAPK pathway. *Crit. Care Med.* **28**, N67–N77 (2000).
8. A. J. Roberts, T. Kon, P. J. Knight, K. Sutoh, S. A. Burgess, Functions and mechanics of dynein motor proteins. *Nat. Rev. Mol. Cell Biol.* **14**, 713–726 (2013).
9. K. J. Verhey, J. W. Hammond, Traffic control: Regulation of kinesin motors. *Nat. Rev. Mol. Cell Biol.* **10**, 765–777 (2009).
10. T. Sato, M. Ishikawa, M. Mochizuki, M. Ohta, M. Ohkura, J. Nakai, N. Takamatsu, K. Yoshioka, JSAP1/JIP3 and JLP regulate kinesin-1-dependent axonal transport to prevent neuronal degeneration. *Cell Death Differ.* **22**, 1260–1274 (2015).
11. H.-J. Nam, R. M. Naylor, J. M. van Deursen, Centrosome dynamics as a source of chromosomal instability. *Trends Cell Biol.* **25**, 65–73 (2015).
12. K. Lee, K. Rhee, PLK1 phosphorylation of pericentrin initiates centrosome maturation at the onset of mitosis. *J. Cell Biol.* **195**, 1093–1101 (2011).
13. M. Magnani, R. Crinelli, M. Bianchi, A. Antonelli, The ubiquitin-dependent proteolytic system and other potential targets for the modulation of nuclear factor-κB (NF-κB). *Curr. Drug Targets* **1**, 387–399 (2000).
14. M. Tafani, B. Pucci, A. Russo, L. Schito, L. Pellegrini, G. A. Perrone, L. Villanova, L. Salvatori, L. Ravenna, E. Petrangeli, M. A. Russo, Modulators of HIF1α and NFκB in cancer treatment: Is it a rational approach for controlling malignant progression? *Front. Pharmacol.* **4**, 13 (2013).
15. R. W. Jackman, M. G. Rhoads, E. Cornwell, S. C. Kandarian, Microtubule-mediated NF-κB activation in the TNF-α signaling pathway. *Exp. Cell Res.* **315**, 3242–3249 (2009).
16. I. Mikenberg, D. Widera, A. Kaus, B. Kaltschmidt, C. Kaltschmidt, Transcription factor NF-κB is transported to the nucleus via cytoplasmic dynein/dynactin motor complex in hippocampal neurons. *PLOS ONE* **2**, e589 (2007).
17. N. Kelkar, C. L. Standen, R. J. Davis, Role of the JIP4 scaffold protein in the regulation of mitogen-activated protein kinase signaling pathways. *Mol. Cell. Biol.* **25**, 2733–2743 (2005).
18. T. Suzuki, I. Tsukamoto, Arsenite induces apoptosis in hepatocytes through an enhancement of the activation of Jun N-terminal kinase and p38 mitogen-activated protein kinase caused by partial hepatectomy. *Toxicol. Lett.* **165**, 257–264 (2006).
19. J. Maranto, J. Rappaport, P. K. Datta, Role of C/EBP-β, p38 MAPK, and MKK6 in IL-1β-mediated C3 gene regulation in astrocytes. *J. Cell. Biochem.* **112**, 1168–1175 (2011).
20. C. M. Lee, Transport of c-MYC by Kinesin-1 for proteasomal degradation in the cytoplasm. *Biochim. Biophys. Acta* **1843**, 2027–2036 (2014).
21. M.-M. Fu, E. L. F. Holzbaur, JIP1 regulates the directionality of APP axonal transport by coordinating kinesin and dynein motors. *J. Cell Biol.* **202**, 495–508 (2013).
22. G. Montagnac, J.-B. Sibarita, S. Loubéry, L. Daviet, M. Romao, G. Raposo, P. Chavrier, ARF6 Interacts with JIP4 to control a motor switch mechanism regulating endosome traffic in cytokinesis. *Curr. Biol.* **19**, 184–195 (2009).
23. T. Akoumianaki, D. Kardassis, H. Polioudaki, S. D. Georgatos, P. A. Theodoropoulos, Nucleocytoplasmic shuttling of soluble tubulin in mammalian cells. *J. Cell Sci.* **122**, 1111–1118 (2009).
24. N. Sylvius, A. Hathaway, E. Boudreau, P. Gupta, S. Labib, P. M. Bolongo, P. Rippstein, H. McBride, Z. T. Bilinska, F. Tesson, Specific contribution of lamin A and lamin C in the development of laminopathies. *Exp. Cell Res.* **314**, 2362–2375 (2008).
25. S. Zitouni, C. Nabais, S. C. Jana, A. Guerrero, M. Bettencourt-Dias, Polo-like kinases: Structural variations lead to multiple functions. *Nat. Rev. Mol. Cell Biol.* **15**, 433–452 (2014).
26. T. Wu, X. Zhang, X. Huang, Y. Yang, X. Hua, Regulation of cyclin B2 expression and cell cycle G_2/m transition by menin. *J. Biol. Chem.* **285**, 18291–18300 (2010).
27. P. Ramkumar, C. M. Lee, A. Moradian, M. J. Sweredoski, S. Hess, A. D. Sharrocks, D. S. Haines, E. P. Reddy, JNK-associated leucine zipper protein functions as a docking platform for Polo-like kinase 1 and Regulation of the Associating Transcription Factor Forkhead box protein K1. *J. Biol. Chem.* **290**, 29617–29628 (2015).
28. B. T. Bajar, E. S. Wang, S. Zhang, M. Z. Lin, J. Chu, A guide to fluorescent protein FRET pairs. *Sensors* **16**, 1448 (2016).
29. I. C. Berke, T. Boehmer, G. Blobel, T. U. Schwartz, Structural and functional analysis of Nup133 domains reveals modular building blocks of the nuclear pore complex. *J. Cell Biol.* **167**, 591–597 (2004).
30. J. Joseph, M. Dasso, The nucleoporin Nup358 associates with and regulates interphase microtubules. *FEBS Lett.* **582**, 190–196 (2008).
31. R.-H. Chou, S.-C. Hsieh, Y.-L. Yu, M.-H. Huang, Y.-C. Huang, Y.-H. Hsieh, Fisetin inhibits migration and invasion of human cervical cancer cells by down-regulating urokinase plasminogen activator expression through suppressing the p38 MAPK-dependent NF-κB signaling pathway. *PLOS ONE* **8**, e71983 (2013).
32. J. M. Kyriakis, J. Avruch, Protein kinase cascades activated by stress and inflammatory cytokines. *Bioessays* **18**, 567–577 (1996).
33. M. D. Galigniana, P. C. Echeverría, A. G. Erlejman, G. Piwien-Pilipuk, Role of molecular chaperones and TPR-domain proteins in the cytoplasmic transport of steroid receptors and their passage through the nuclear pore. *Nucleus* **1**, 299–308 (2010).
34. L. Wang, R. Payton, W. Dai, L. Lu, Hyperosmotic stress-induced ATF-2 activation through Polo-like kinase 3 in human corneal epithelial cells. *J. Biol. Chem.* **286**, 1951–1958 (2011).
35. C. Xie, L. Fu, N. Liu, Q. Li, Overexpression of SPAG9 correlates with poor prognosis and tumor progression in hepatocellular carcinoma. *Tumour Biol.* **35**, 7685–7691 (2014).
36. J. H. Ha, M. Yan, R. Gomathinayagam, M. Jayaraman, S. Husain, J. Liu, P. Mukherjee, E. P. Reddy, Y. S. Song, D. N. Dhanasekaran, Aberrant expression of JNK-associated leucine-zipper protein, JLP, promotes accelerated growth of ovarian cancer. *Oncotarget* **7**, 72845–72859 (2016).
37. D. Kanojia, M. Garg, S. Gupta, A. Gupta, A. Suri, Sperm-associated antigen 9 is a novel biomarker for colorectal cancer and is involved in tumor growth and tumorigenicity. *Am. J. Pathol.* **178**, 1009–1020 (2011).
38. H. K. Koul, M. Pal, S. Koul, Role of p38 MAP kinase signal transduction in solid tumors. *Genes Cancer* **4**, 342–359 (2013).
39. H.-Y. Yong, M.-S. Koh, A. Moon, The p38 MAPK inhibitors for the treatment of inflammatory diseases and cancer. *Expert Opin. Investig. Drugs* **18**, 1893–1905 (2009).
40. E. Schreiber, P. Matthias, M. M. Muller, W. Schaffner, Rapid detection of octamer binding proteins with 'mini-extracts', prepared from a small number of cells. *Nucleic Acids Res.* **17**, 6419 (1989).
41. Y. Zheng, M. L. Wong, B. Alberts, T. Mitchison, Nucleation of microtubule assembly by a γ-tubulin-containing ring complex. *Nature* **378**, 578–583 (1995).
42. A. Kumar, C. M. Lee, E. P. Reddy, c-Myc is essential but not sufficient for c-Myb-mediated block of granulocytic differentiation. *J. Biol. Chem.* **278**, 11480–11488 (2003).

Acknowledgments: We thank P. K. Datta, T. L. Schwarz, E.L.F. Holzbaur, K. S. Lee, K. Yoshioka, and A. Miyawaki for the gifts of expression plasmids; E. P. Reddy, S. C. Cosenza, S. J. Baker, Y. K. Lieu, S. Jatiani, R. Ang, NYCTC, S. Y. Yip, and S. D. Gloria for their support, reagents, suggestions, and critical reading of the manuscript. **Funding:** Confocal and STED microscopy was performed at the Microscopy CoRE at the Icahn School of Medicine at Mount Sinai, supported with funding from the NIH Shared Instrumentation Grant (FAIN: S10OD021838).
Author contributions: C.M.L. designed the studies, performed the experiments, analyzed the data, and wrote the paper. K.A. performed the experiments on the nuclear JLP. J.J. performed the experiments to identify the CLD of JLP. S.K.P.K. collaborated in the experiments using the shRNA methodology. R.J. identified the CLD of JLP and collaborated in the experiments involving the CLD mutants. **Competing interests:** The authors declare that they have no competing interests. **Data and materials availability:** The expression plasmid Venus/pCS2 can be provided by A. Miyawaki pending scientific review and a completed material transfer agreement. Requests for the expression plasmid Venus/pCS2 should be submitted to A. Miyawaki at the RIKEN Brain Science Institute. All data needed to evaluate the conclusions in the paper are present in the paper and/or the Supplementary Materials. Additional data related to this paper may be requested from the authors.

Submitted 7 August 2018
Accepted 18 July 2019
Published 28 August 2019
10.1126/sciadv.aav0318

Citation: C. M. Lee, K. Aizawa, J. Jiang, S. K. Kung, R. Jain, JLP-centrosome is essential for the microtubule-mediated nucleocytoplasmic transport induced by extracellular stimuli. *Sci. Adv.* **5**, eaav0318 (2019).